

MATRIX DESIGN OF A NOVEL DUCTILE CAST IRON MODIFIED BY W AND Al: A COMPARISON BETWEEN THERMODYNAMIC MODELING AND EXPERIMENTAL DATA

Gülşah Aktaş Çelik^{1}, Maria-Ioanna T. Tzini², Şeyda Polat¹,
Ş. Hakan Atapek¹, Gregory N. Haidemenopoulos^{2,3}*

¹*Kocaeli University, Department of Metallurgical and Materials Engineering, Kocaeli, Turkey*

²*University of Thessaly, Department of Mechanical Engineering, Volos, Greece*

³*Khalifa University of Science & Technology, Department of Mechanical Engineering, UAE*

Received 17.10.2019

Accepted 02.03.2020

Abstract

In high-temperature applications of ferrous materials, as in the case of exhaust manifolds, high thermal and mechanical stability are required. Stainless steels and Ni-resist alloys having austenitic matrices are good candidates to meet these requirements at elevated temperatures; however, they are expensive materials and present difficulties in casting. Ferritic ductile cast irons, like the commercial SiMo alloy, are comparatively cheaper materials with better castability, but they cannot be used above approximately 800 °C. Thus, to meet the requirements with low-cost materials having improved high-temperature properties, new alloys must be developed by ferrite forming elements having the potential to increase equilibrium temperature. In this study, initially, a novel ductile cast iron matrix was designed using 1 W and 0-4 Al wt.-% and their phases stable at room temperature, transformation temperatures, solidification sequences and thermal expansivity values were determined using thermodynamic calculations with ThermoCalc software. Computational studies revealed that (i) designed alloy matrices had graphite and M₆C type carbides embedded in a ferritic matrix at room temperature as expected, (ii) A₁ temperature increased as aluminum content increased. The obtained values were all above that of commercial SiMo alloy, (iii) the detrimental effect of increased aluminum addition on graphite content, and thermal expansivity was observed. Secondly, microstructural and thermal characterizations of cast alloys were performed for validation – the obtained data were in good agreement with the thermodynamic calculations.

*Corresponding author: Gülşah Aktaş Çelik, gulsahaktas@gmail.com

Keywords: alloy design; Thermo-Calc; ductile cast iron; microstructure; characterization.

Introduction

Exhaust manifolds deliver hot and oxidative exhaust gases from the combustion chamber to the atmosphere [1, 2]. Initial exhaust manifolds were manufactured using unalloyed high carbon grey cast irons that could be used at operating temperatures up to 540 °C [3]. Due to the increase in the power density of new engines, manufacturers are in search of new materials for exhaust manifolds that can withstand temperatures above 950 °C [4-8]. Such materials must have high thermal conductivity, high oxidation resistance, low thermal expansion coefficient and mechanical stability at elevated temperatures [3]. Austenitic stainless steels and austenitic ductile cast irons (Ni-resist alloys) are good candidates to meet these requirements [6-8]. However, they are expensive materials and present difficulties in casting due to high solidification temperatures [9]. The SiMo cast irons having a ferritic matrix are comparatively cheaper materials with better castability [4, 10]. Besides, the ferritic matrix provides higher thermal conductivity and lower thermal expansion coefficient compared to the austenitic one [3]. High thermal conductivity provides fast cooling; thus, the material is subjected to high temperatures for shorter periods [11, 12]. Low thermal expansion coefficient is vital for long service life avoiding cracks that may form due to thermal fatigue [4, 13]. Despite all the mentioned qualities, ferritic ductile cast irons cannot be used above their transformation temperature from austenite to ferrite (A_1) which limits their use above approximately 800 °C [14]. Thus, it will be beneficial to increase A_1 temperature by using modification elements like Si, Nb, W, Al, Cr etc. [15]. On the other hand, it is essential to consider the effect of alloying elements on graphite distribution and morphology since it directly affects the mechanical and thermal properties. Despite providing the best mechanical properties, spheroidal graphite exhibits lower conductivity than vermicular and flake graphite [11-13, 16-18]. According to the literature, Si and Al promote the graphite formation and increase nodule count as well as stabilize ferrite due to their high solubility in that phase [19-21]. Alloying elements like Al [22], Ti [23], and Nb [24] affect the graphite morphology by changing it from spheroidal to vermicular. Mechanical properties are also affected by the addition of alloying elements. Some carbide forming elements (such as Mo, W, and Nb) can be added in small quantities (up to 1 wt.-%) to improve mechanical properties since these elements provide precipitation strengthening by carbides and also prevent grain boundary motion and refine grain size [8, 24-26]. In this study, a novel ductile cast iron composition 3.5C, 4Si, 1W wt.-% was selected as the main composition. In order to obtain a hypereutectic composition which is useful for casting and solidification, carbon and silicon amounts determining the carbon equivalent were selected as 3.5 and 4 wt.-%, respectively. In the designed matrix, tungsten was used instead of molybdenum, since tungsten is both ferrite and carbide forming element and provides oxidation resistance. In order to increase the A_1 temperature, aluminum additions up to 4 wt.-% were made to the main composition since higher aluminum levels are known to affect the graphite morphology adversely [22], and therefore thermal properties [16-18]. Thermodynamic calculations on these compositions were carried out employing Thermo-Calc software and the results were validated by experimental studies to investigate the possibility of their use in place of commercial ferritic ductile cast irons at more demanding working conditions.

Experimental work

Thermodynamic calculations for the composition of 3.5 C, 4 Si, 1 W, 0-4 Al (wt.-%) were carried out with Thermo-Calc software. The TCFE6 database was used in order to determine A_1 temperatures of the studied compositions, the mole fraction of graphite, phases stable at room temperature (RT), and thermal expansivity of ferrite. Solidification sequences of the compositions were studied using the Scheil module.

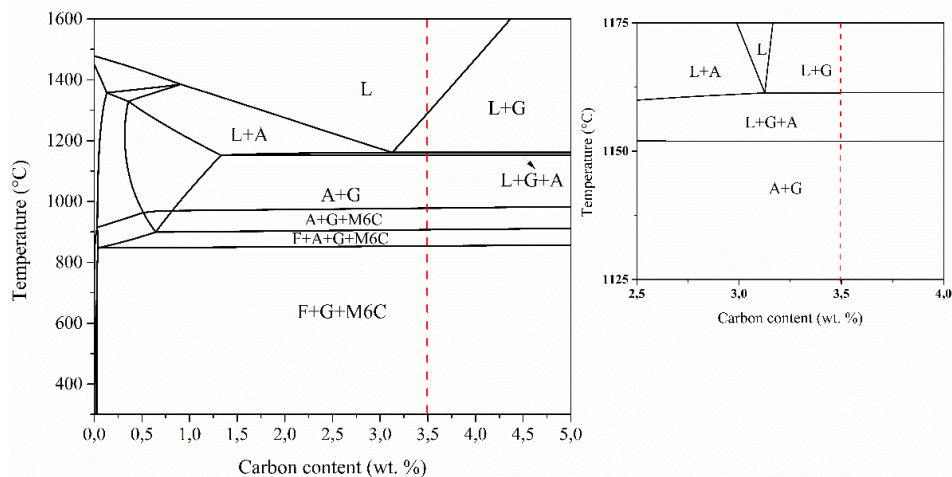
After calculations, in order to validate the computed values, 3.5C-4Si-1W- x Al alloys (wt.-%) were produced as Y block by sand mold casting, according to ASTM A 536-84 standard. For this process, 5 kg charge was prepared with nodular pig iron (MMM International Trading Co., 4.30C-0.7Si-0.06Mn-0.05P-0.018S wt.-%), ferrosilicon (MMM International Trading Co., 72Si-1.50Al-0.10C-0.02S-0.024P wt.-%), ferrotungsten (70W-0.5Mn-1Si-0.06S-0.25C wt.-%) and DIN 1020 steel. The used materials for the charge were all commercial materials. The charge was melted in the 35 kW Inductotherm induction furnace with a capacity of 25 kg. Just before the melting process was completed, pure aluminum was added according to the chosen composition. The melting process was completed at 1560 °C, followed by spheroidization process which was carried out in a SiC crucible. For spheroidization process, the nucleation agent (FerroPem, 75Si-0.94Ca-1.68Ce-0.89Al wt.-%) and magnesium-rich alloy FeSiMg (Snam Alloys Pvt. Ltd., 45Si-7Mg-0.56Al-1.15Ca-1.18R wt.-%, R : rare earth) for spheroidization were put at the bottom of the crucible before pouring the charge. A sample from the molten alloy, after spheroidization, was taken by pouring it into a copper mold, in order to verify the chemical composition by optical emission spectrometer (OES, Foundry Master) and then the rest of the molten metal was cast into the sand mold. In order to specify the cast alloys, systematic coding is preferred. In the coding system, the main composition (3.5C, 4Si, 1W wt.-%) is coded as specimen 0Al and the others are coded as 1Al, 2Al, 3Al and 4Al for 1, 2, 3 and 4 wt.-% Al additions, respectively.

Both microstructural examinations and thermal analyses were applied to the cast alloys in order to validate the computational results in terms of (i) formation of the phases during solidification, (ii) critical temperatures, and (iii) phases stable at RT. For microscopic examinations, as-cast alloys were prepared by metallographic methods. Microstructural characterization was carried out using both light microscope (LM, Olympus BX41M-LED), scanning electron microscope (SEM, Jeol JSM 6060) and energy dispersive spectrometer (EDS, IXRF). Phases present were also identified by x-ray diffraction (XRD, Rigaku Ultima+). XRD studies were carried out with Cu- K_α radiation and a scanning speed of 1.0 °/min. The determined phases were quantified according to ISO 945-2, by an image analyzer (IA, Leica Las V4.12). Thermal analysis was carried out by using a differential thermal analyzer (DTA, Netzsch STA 409 PG Luxx). The DTA tests were carried out under vacuum, Al_2O_3 crucibles were used and a calibration was performed as follows: (i) heating to 1460 °C at a rate of 5 °C. min⁻¹, (ii) holding at that temperature for 5 min, (iii) cooling to RT at a rate of 5 °C.min⁻¹. The samples were tested under these conditions and an empty crucible was used as reference material.

Results and discussion

Thermodynamic modeling

Carbon isopleth concerning a constant 4Si1W composition (0Al) is given in Figure 1a, confirming the composition containing 3.5% C is hypereutectic. Since some of the phase areas are very narrow in this isopleth, expanded drawings are also illustrated in the same figure. Solidification starts with graphite (G) precipitation from the liquid phase (L) and finishes after austenite (A) transformation. M_6C carbide starts precipitating at 978 °C. Ferrite (F) transformation from austenite starts at 907 °C and finishes at 853 °C. The stable phases at room temperature appear to be ferrite, graphite and M_6C . In order to understand the effect of aluminum addition on austenite to ferrite phase transformation, aluminum isopleth of 3.5C4Si1W constant composition is given in Figure 1b. According to this isopleth, the phase transformation sequence remains the same up to 2.7 Al wt.-%. At higher aluminum additions above this composition, ferrite formation from austenite occurs rather than M_6C precipitation. However, the final microstructure at RT does not change and consists of ferrite, graphite and M_6C up to the studied highest aluminum addition. On the other hand, all the transformation temperatures except for the precipitation of M_6C are increased by increasing aluminum content.



(a)

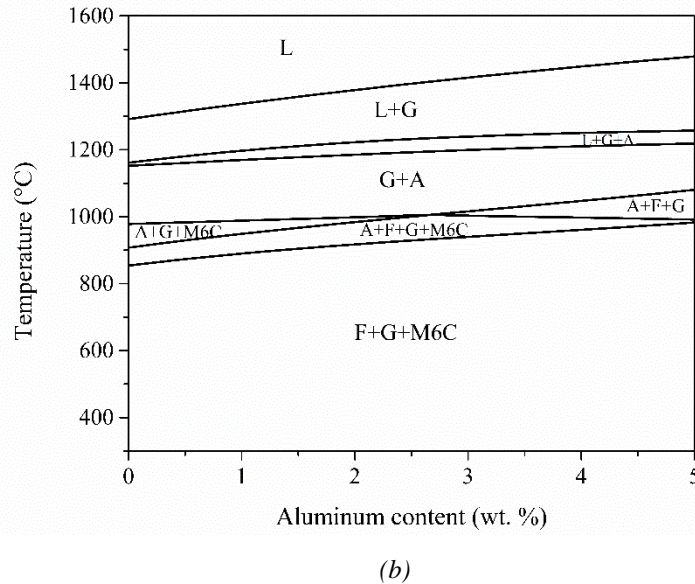
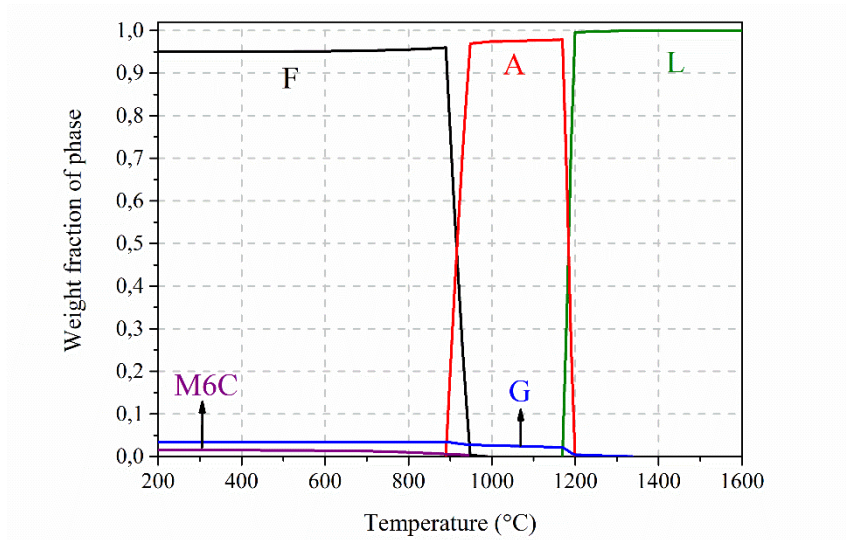


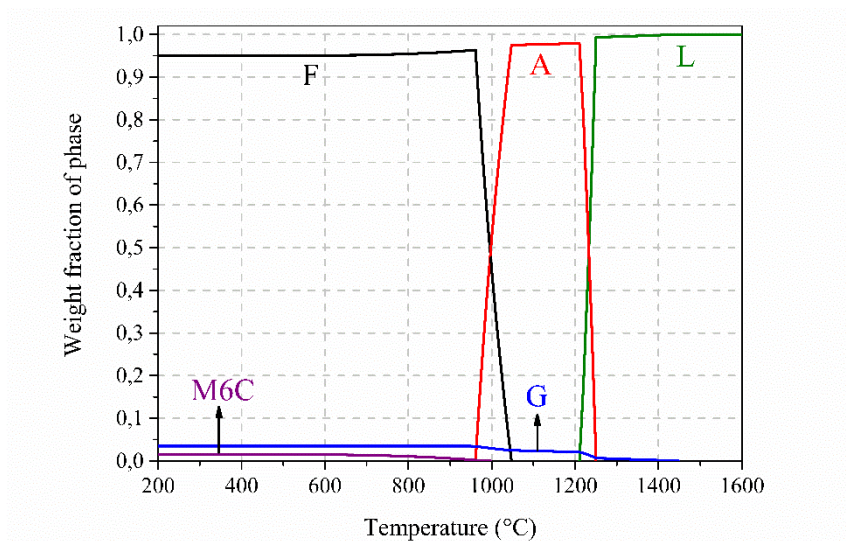
Fig. 1. (a) C isopleth for 0Al alloy and (b) Al isopleth sections.

Thermo-Calc software also provides the amounts of phases for the studied compositions as a function of temperature, and the data for 1Al and 4Al are presented in Figure 2 in order to reveal the effect of aluminum addition on amounts of austenite, ferrite, carbide and graphite. It is important to understand the effect of aluminum addition on A_1 temperature in order to determine the maximum service temperature of the compositions. Figure 3 shows the variation of A_1 temperature as a function of aluminum content and the curve clearly indicates that aluminum addition increases the A_1 temperature. While A_1 temperature of an alloy having no aluminum (0Al) is 853 °C, it is increased to 960 °C by the addition of 4 Al wt.-%. This effect is also reported in dilatometric data of 3.4C-3Si-0.45Mo and 3.1C-3.1Si-0.55Mo-3Al (wt.-%) alloys studied by *Ibrahim et al.* and they concluded that A_1 temperature was raised by 110 °C and reached to 960 °C due to the solubility of aluminum within the ferrite lattice [25].

In calculations, the variation of graphite content as a function of aluminum addition is also studied, and the obtained data is given in Figure 4. The diagram clearly shows that aluminum has a decreasing effect on graphite content. In solidified cast irons, not only segregation but also the accumulation of aluminum atoms around the graphite phases causes nonhomogeneous diffusion of carbon results in a change in the morphology of graphite and its content [25]. Thermal expansivity is another design criterion for the materials used in high-temperature applications and it must be kept low. However, calculations indicated that the thermal expansivity of ferrite at RT increases with aluminum addition (Figure 5).



(a)



(b)

Fig. 2. Variation of the weight fraction of phases as a function of temperature; (a) 1Al and (b) 4Al.

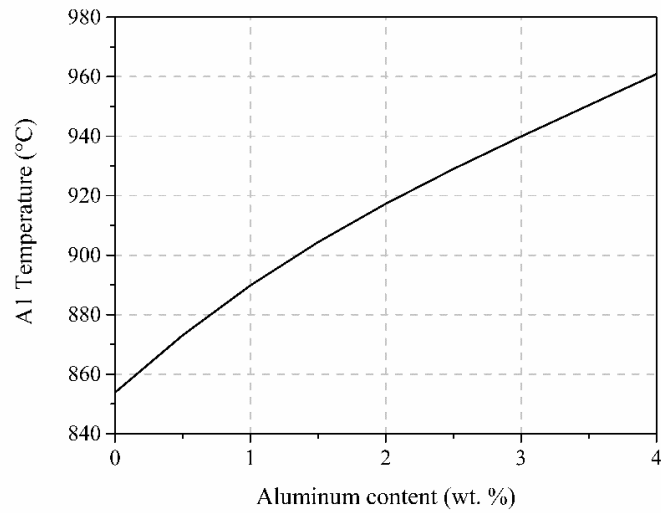


Fig. 3. Change in A_1 temperature as a function of aluminum addition.

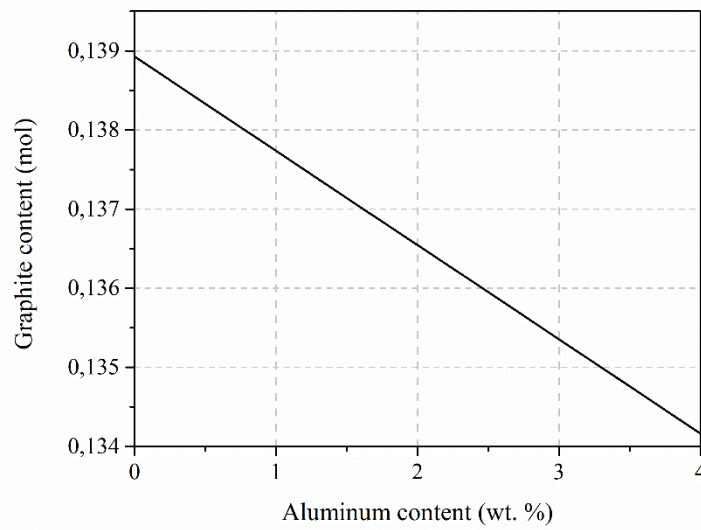


Fig. 4. Change of graphite content as a function of aluminum addition.

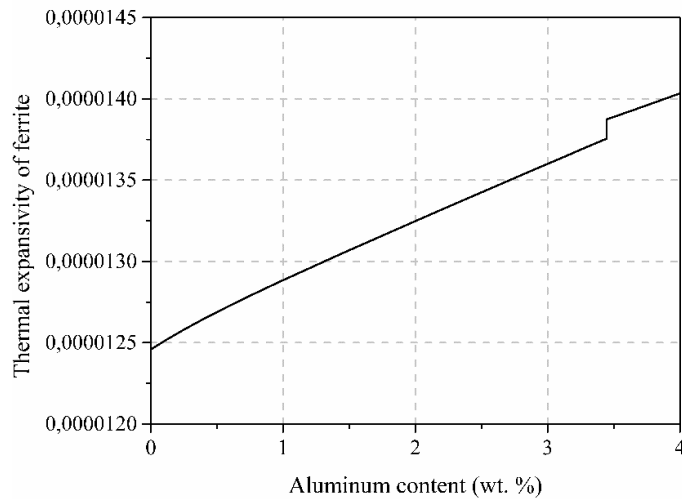


Fig. 5. Change in thermal expansivity of ferrite at RT with aluminum addition.

Solidification sequences of the studied compositions are given in Figure 6. Solidification starts with graphite precipitation and is completed by austenite transformation. Figure 6 also denotes that the solidification temperature changes from 1292 °C to 1450 °C with aluminum additions from 0 to 4 wt.-%.

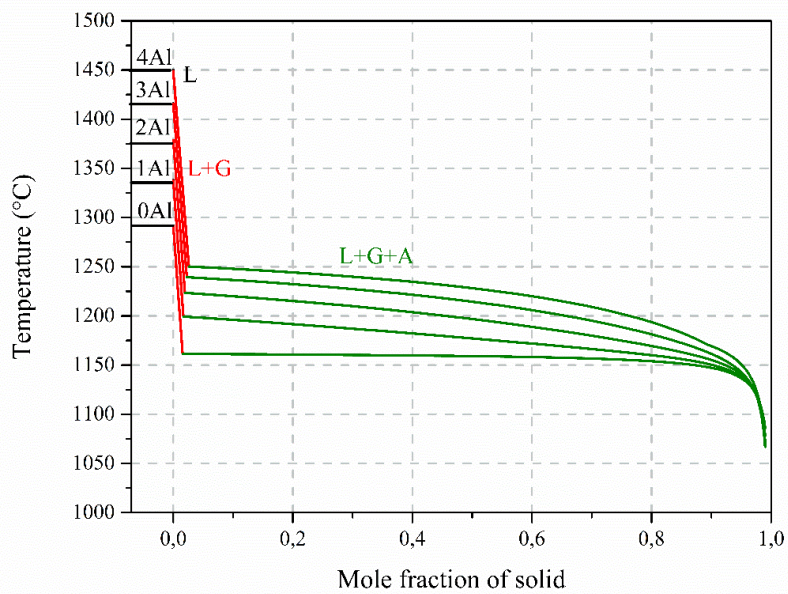


Fig. 6. Solidification paths of 3.5C-4Si-1W-xAl alloys.

All transformation temperatures of the alloys, calculated by Thermo-Calc studies, are given in Table 1. The notations for the temperatures are as follows: T_G indicates the start temperature of graphite precipitation from the liquid phase that also denotes the start of solidification, T_{AS} indicates the start temperature of austenite formation from the liquid phase, T_{AF} indicates the finish temperature of austenite formation also denoting the completion of solidification, T_F indicates the start temperature of ferrite, and T_{M6C} indicates the start temperature M_6C carbide precipitation. The calculated values indicate that all transformation temperatures shift to higher values by aluminum addition.

Table 1. Critical temperatures of cast irons calculated by Thermo-Calc studies ($^{\circ}C$).

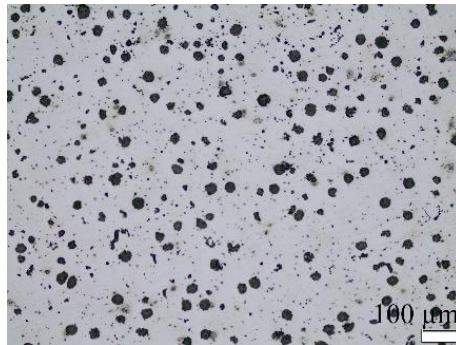
Alloy	T_G	T_{AS}	T_{AF}	T_F	T_{M6C}	A_1
0Al	1292	1161	1085	907	978	853
1Al	1338	1199	1077	950	988	889
2Al	1379	1223	1070	985	998	917
3Al	1416	1239	1137	1017	1002	939
4Al	1450	1250	1170	1048	997	960

Microstructural characterization

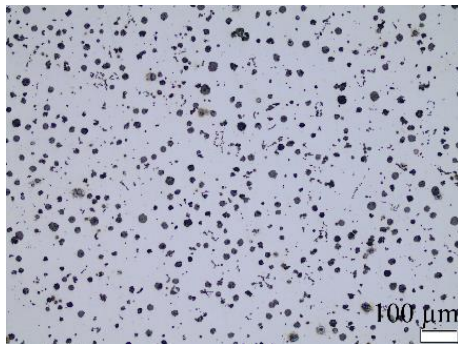
Before microstructural characterization, the chemical compositions of fully solidified cast alloys were determined by OES. Table 2 shows the chemical compositions of the cast alloys and they are in the required range as designed. The LM images of the polished cast samples are given in Figure 7 to investigate the graphite content and morphology. The quantified data by image analysis are given in Figure 8 and Table 3. According to Figure 8, as aluminum content increases, graphite content (area %) decreases and similar results were obtained by Thermo-Calc calculations. The graphite morphology changes from spheroidal (VI) to irregular spheroidal (V) and vermicular (III) as aluminum content increases (Table 3). These results are in agreement with the current literature in terms of the aluminum effect on the graphite morphology in ductile cast irons [22]. *Ibrahim et al.* presented that the addition of 3 wt.-% Al to SiMo ductile cast iron decreased the nodularity of graphite. Due to non-homogeneous and irregular accumulation of aluminum around the graphite nodules, a non-uniform diffusion of carbon is revealed resulting in deformed graphite morphology [25]. Lithium also emphasizes this effect and the reported data suggested that the deterioration effect of aluminum could be decreased by using a nodularizer combining magnesium with rare earth metals in the melt treatment [27].

Table 2. Chemical compositions of the cast alloys obtained by OES (wt.-%).

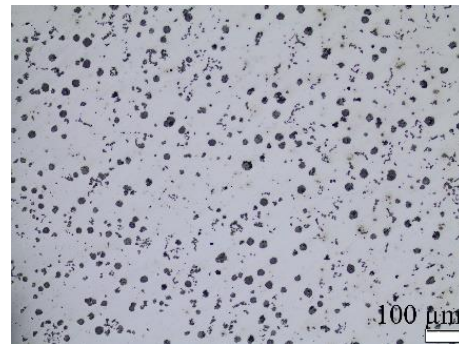
Alloy	C	Si	W	Al	Mg	Mn	P	S
0Al	3.57	4.04	0.96	0.02	0.074	0.231	0.0579	0.0282
1Al	3.46	3.96	0.97	0.97	0.082	0.235	0.0597	0.0285
2Al	3.47	3.99	1.03	2.03	0.078	0.245	0.0572	0.0321
3Al	3.52	4.07	1.02	3.05	0.081	0.225	0.0581	0.0287
4Al	3.54	4.05	1.04	4.03	0.079	0.228	0.0558	0.0355



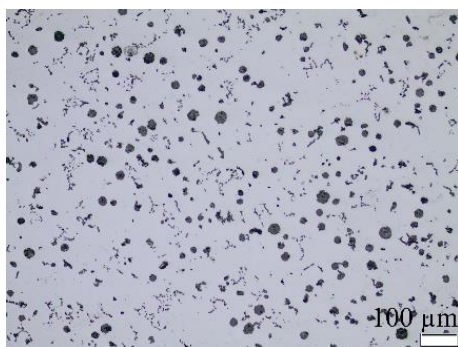
(a)



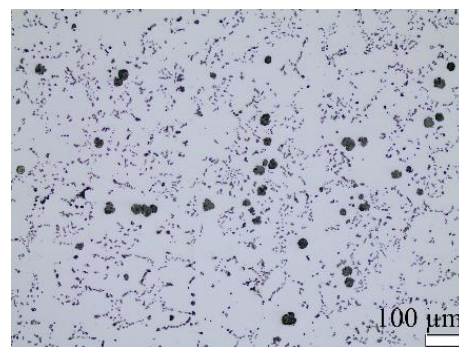
(b)



(c)




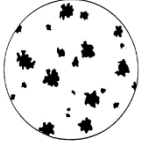
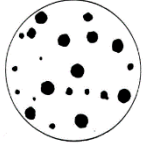
(d)



(e)

Fig. 7. LM images showing the graphite morphology in polished cast irons (a) 0Al, (b) 1Al, (c) 2Al, (d) 3Al and (e) 4Al.

Table 3. Image analysis results for graphite morphology as determined by DIN EN ISO 945-2 (area %).

Alloy	III 	V 	VI 	Others
0Al	6.0	49.6	40.7	3.7
1Al	8.6	40.3	46.5	4.6
2Al	15.0	45.3	32.1	7.6
3Al	15.1	41.7	36.6	6.6
4Al	20.7	41.3	25.5	12.5

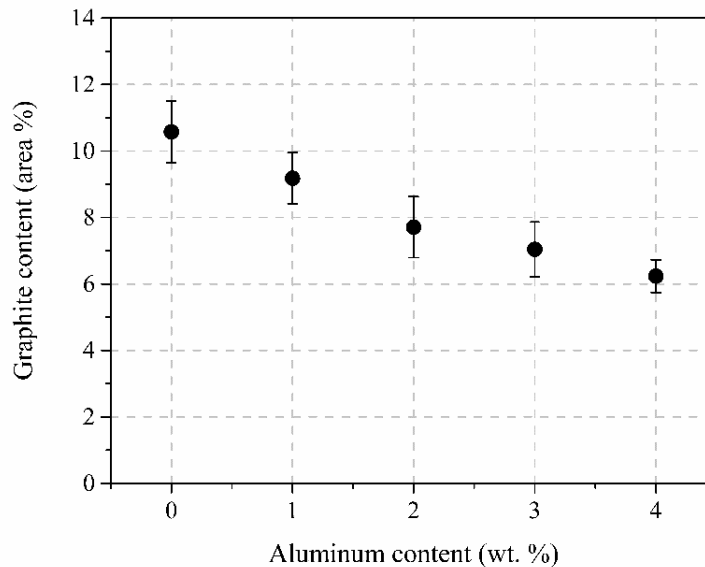


Fig. 8. Change of the graphite content by aluminum addition.

The microstructures of 0Al and 4Al are given in Figure 9. The microstructural features of the studied alloys consist of graphite, pearlite, coarse and skeleton-like carbides embedded in the ferritic matrix. In order to clarify the details of the pearlite region and coarse carbides within the matrix of 0Al, an SEM image at higher magnification is inserted in Figure 9a. Such pearlitic formations can be seen in cast irons like SiMo ductile cast alloys [25, 28, 29] having similar C and Si contents as 0Al. However, since aluminum addition prohibits the formation of pearlite [25], not only the amount of pearlite decrease but also its lamellar morphology changes to a structure having

dispersed cementite. This effect was observed in the microstructure of 4Al as seen in Figure 9b. EDS analyses of coarse carbides revealed the composition as 61.2W-17.9C-17.3Fe-3.6Si wt.-% indicating that they were W_6C carbides. In order to confirm the phases, XRD studies were carried out and the data for 0Al and 4Al are given in Figure 10 and XRD spectra validate all phases present in the microstructure.

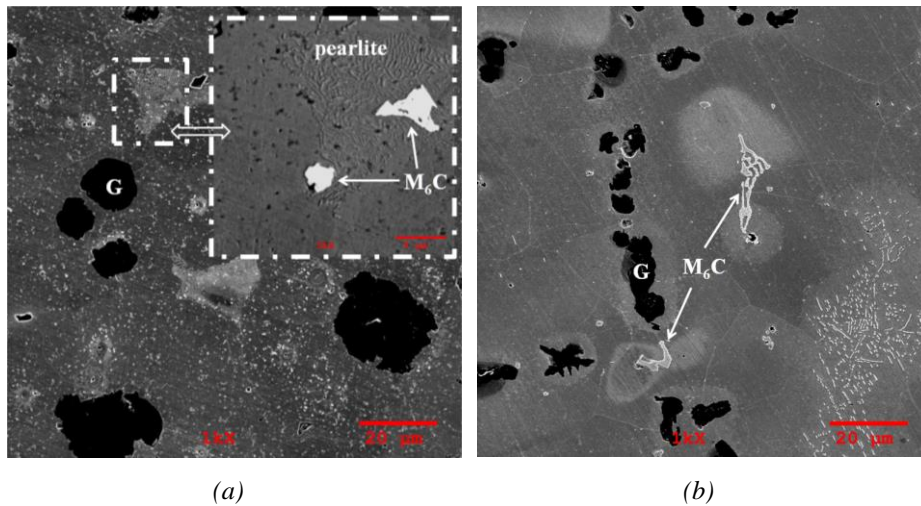


Fig. 9. SEM images showing the microstructure of the cast alloys; (a) 0Al and (b) 4Al.

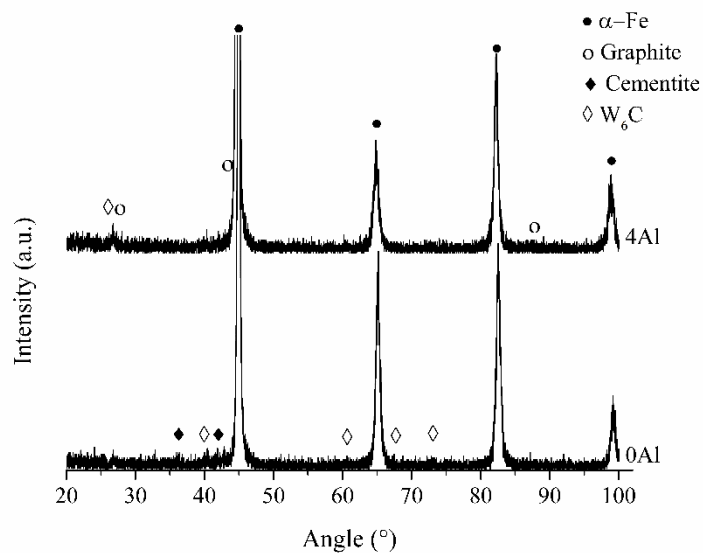


Fig. 10. XRD patterns 0Al and 4Al cast irons.

Evaluation of phase transformations by DTA

The DTA data indicating the transformation temperatures for the heating condition is given in Figure 11 and resulting data are tabulated in Table 4. In the DTA thermogram, the results only for the specimens 0Al, 2Al and 4Al are given for clarity and the others show similar behavior. The notations for temperatures given in Table 4 are the same as the ones in Table 2. The DTA results indicate that all transformation temperatures shift towards higher temperatures and A_1 temperature reaches as high as 981 °C for the highest aluminum addition. Thermo-Calc data (Table 2) indicated the same trend as DTA results (Table 4) and the calculated temperatures (CT) were close to those observed by thermal analysis. The small discrepancy between the calculated and measured temperatures could be since actual compositions of the cast alloys include Mn, Mg, P, S, and other trace elements that do not exist in the Thermo-Calc calculations.

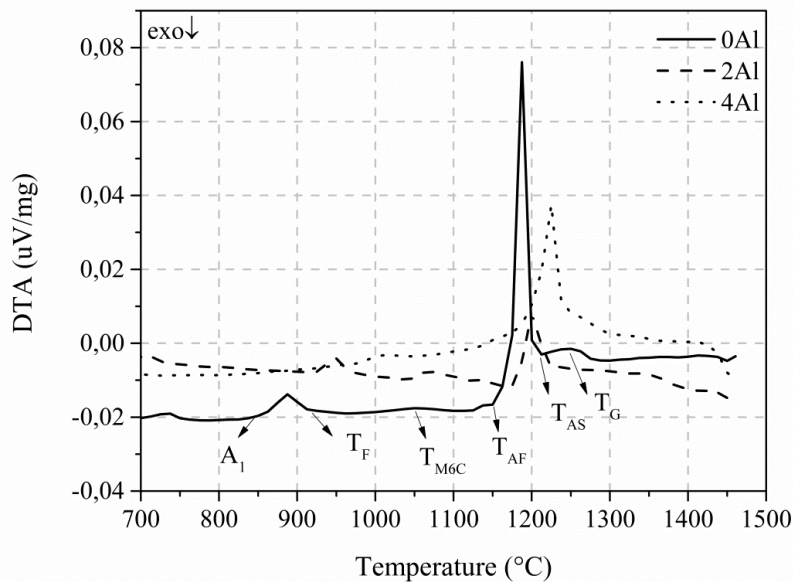


Fig. 11. Thermogram of the cast irons upon heating for 0Al, 2Al, 4Al.

Table 4. Critical temperatures of cast irons identified by calculations and DTA analyses (°C).

Alloy	T_G		T_{AS}		T_{AF}		T_F		T_{M6C}		A_1	
	CT	DTA	CT	DTA	CT	DTA	CT	DTA	CT	DTA	CT	DTA
0Al	1292	1247	1161	1195	1085	1180	907	908	978	1053	853	863
1Al	1338	1343	1199	1206	1077	1187	950	946	988	1050	889	905
2Al	1379	1333	1223	1221	1070	1185	985	964	998	1071	917	931
3Al	1416	1350	1239	1224	1137	1196	1017	974	1002	1056	939	940
4Al	1450	1402	1250	1237	1170	1209	1048	1114	997	1053	960	981

Conclusion

In this study, thermodynamic calculations with Thermo-Calc software on novel ductile cast iron compositions 3.5C-4Si-1W- x Al where x varies between 0 – 4 (wt. %) were carried out and results were validated by experimental studies on cast samples to reveal the possibility of its use in place of commercial ferritic ductile cast irons at more demanding working conditions. Thermo-Calc calculations revealed that; (i) the stable phases at RT were ferrite, graphite and M_6C carbide for all compositions, (ii) with increasing aluminum additions, A_1 temperature increased, graphite content decreased and thermal expansivity increased, (iii) according to the solidification sequence, solidification started with graphite precipitation for all compositions however it is completed by austenite transformation for 0, 1, 2 wt. % Al, whereas by ferrite transformation for 3 and 4 wt. % Al. Experimental studies showed that; (i) the stable phases at RT were ferrite, graphite and W_6C carbide for all aluminum added compositions as indicated by Thermo-Calc, (ii) graphite content decreased by aluminum addition as indicated by calculations and its morphology changed from spheroidal to vermicular and (iii) A_1 temperatures increased as aluminum increased in heating thermograms and they were very close to those calculated by Thermo-Calc.

Acknowledgment

The authors, G. Aktaş Çelik, Ş. Polat and Ş. H. Atapek, wish to acknowledge the financial support given by the Scientific Research Projects Coordination Unit of Kocaeli University under the project no 2017/118.

References

- [1] A. A. Partoaa, M. Abdolzadeh, M. Rezaeizadeh: J Cent South Univ, 24 (2017) 546–559.
- [2] [G.M. Castro Güizaa, W. Hormaza, A.R. Galvis E, L.M. Méndez Moreno: Eng Fail Anal, 82 (2017) 138–148.
- [3] Y. Zhang, M. Li, L. A. Godlewski, J. W. Zindel, Q. Feng: Metall Mater Trans A, 47A (2016) 3289-3294.
- [4] M. Ekström, S. Jonsson: Mater Sci Eng, A 616 (2014) 78–87.
- [5] M. Ekström, P. Szakalos, S. Jonsson: Oxid Met, 80 (2013) 455–466.
- [6] F. Tholence, M. Norell: Oxid Met, 69 (2008) 37–62.
- [7] J. P. Shingledecker, P. J. Maziasz, N. D. Evans, M. J. Pollard: Int J Press Vessels Pip, 84 (2007) 21–28.
- [8] Y. Zhang, M. Li, L. A. Godlewski, J. W. Zindel, Q. Feng: Mater Charact, 139 (2018) 19–29.
- [9] H. Inoue, T. Koseki: Acta Mater, 124 (2017) 430-436.
- [10] M. Górný: Arch Foundry Eng, 8:3 (2008) 59-64.
- [11] D. Holmgren, A. Diószegi, I. L. Svensson: Int J Cast Met Res, 20:1 (2007) 30-40.
- [12] Z.J. Ma, D. Tao, Z. Yang, Y.C. Guo, J.P. Li, M.X. Liang, L. T. Li Yeung: Materials and Design, 93 (2016) 418–422.
- [13] X Wu, G. Quan, R. Macneil, Z. Zhang, X. Liu, C. Sloss: Metall Mater Trans A, 46:6 (2015) 2530–2543.
- [14] L. M. Åberg, C. Hartung: Trans Indian Inst Met: 65:6 (2012) 633–636.
- [15] G. E. Totten, Steel Heat Treatment, second ed. Portland, Longman, New York, 2006.

- [16] A. I. Al-Ghonamy, M. Ramadan, N. Fathy, K. M. Hafez, A. A. El-Wakil: *Int J Civil & Env Eng IJCEE-IJENS*, 10:03 (2010) 1-5.
- [17] H. Nakayama, B.-R. Zhao, N. Furusato, S. Yamada, T. Nishi, H. Ohta: *Mater Trans*, 59: 3 (2018) 412-419.
- [18] T. Sjögren, I. L. Svensson: *Metall Mater Trans A*, 38:4 (2007) 840-847.
- [19] R. González-Martínez, U. de la Torre, J. Lacaze, J. Sertuch: *Mater Sci Eng A*, 712 (2018) 794–802.
- [20] N. Haghdadi, B. Bazaz, H.R. Erfanian-Naziftoosi, and A.R. Kiani-Rashid: *Int J Miner Metall Mater*, 19:9 (2012) 812-820.
- [21] A. Shayesteh-Zeraati, H. Naser-Zoshki, A.R. Kiani-Rashid: *J Alloys Compd*, 500 (2010) 129–133.
- [22] M.S. Sołński, A. Jakubus, G. Stradomski: *Arch Foundry Eng*, 13:2 (2013) 163-168.
- [23] M. Górny and M. Kawalec: *J Mater Eng Perform*, 22:5 (2013) 1519-1524.
- [24] T. N. F. Souza, R. A. P. S. Nogueira, F. J. S. Franco, M. T. P. Aguiar, P. R. Cetlin: *Mat Res*, 17:5 (2014) 1167-1172.
- [25] M. M. Ibrahim, A. Nofal, M.M. Mourad: *Metall and Mater Trans B*, 48:2 (2017) 1149-1157.
- [26] A. Alhussein, M. Risbet, A. Bastien, J. P. Chobaut, D. Balloy, J. Favergeon: *Mater Sci Eng A*, 605 (2014) 222–228.
- [27] D. Li: *Metall and Mater Trans B*, 49B (2018) 858-859.
- [28] P. Matteis, G. Scavino, A. Castello, D. Firrao: *Procedia Mater Sci*, 3 (2014) 2154 – 2159.
- [29] B. Cygan, M. Stawarz, J. Jezierski: *Arch Foundry Eng*, 18-4 (2018) 103-109.



Creative Commons License

This work is licensed under a Creative Commons Attribution 4.0 International License.